

Soil moisture modelling with ERA5-Land retrievals, topographic indices and in-situ measurements and its use for predicting ruts

Marian Schönauer¹, Anneli M. Ågren², Klaus Katzensteiner³, Florian Hartsch¹, Paul Arp⁴, Simon Drollinger⁵, Dirk Jaeger¹

¹Department of Forest Work Science and Engineering, University of Göttingen, Göttingen, Germany

²Department of Forest Ecology and Management, Swedish University of Agricultural Sciences, Umeå, Sweden

³Institute of Forest Ecology, University of Natural Resources and Life Sciences, Vienna, Vienna, Austria

⁴Forestry and Environmental Management, University of New Brunswick, New Brunswick, Canada

⁵Department of Physical Geography, University of Göttingen, Göttingen, Germany

Correspondence to: Marian Schönauer (marian.schoenauer@uni-goettingen.de)

Abstract

Spatiotemporal modelling is an innovative way of predicting soil moisture and has promising applications in supporting sustainable forest operations. One such application is the prediction of rutting, since rutting can cause severe damage to forest soils and ecological functions.

In this work, we used ERA5-Land soil moisture retrievals and several topographic indices to model variations of in-situ soil water content, by means of a random forest model. We then correlated the predicted soil moisture with rut depth from different trials.

Our spatiotemporal modelling approach successfully predicted soil moisture with a Kendall's rank correlation coefficient of 0.62 (R^2 of 64%). The final model included the spatial depth-to-water index, topographic wetness index, stream power index, as well as temporal components such as month and season, and ERA5-Land soil moisture retrievals. These retrievals showed to be the most important predictor in the model, indicating a large temporal variation. The prediction of rut depth was also successful, resulting in a Kendall's correlation coefficient of 0.61.

Our results demonstrate that by using data from several sources, including ERA5-Land retrievals, topographic indices and in-situ soil moisture measurements, we can accurately predict soil moisture and use this information to predict rut depth. This has practical applications in reducing the impact of heavy machinery on forest soils and avoiding wet areas during forest operations.

Keywords: spatiotemporal modelling, forest management, forest engineering, rutting, downscaling, reanalysis

1 Introduction

For decades, forestry research has sought solutions to accurately predict the trafficability of forest soils (Mattila and Tokola, 2019; White et al., 2012; Murphy et al., 2007). In order to further sustainable forest management, efficient protection of forest soils is mandatory (Vega-Nieva et al., 2009; Picchio et al., 2020; Uusitalo et al., 2019). Heavy harvesting and forwarding machines have been frequently associated with severe soil damage, particularly when operating on soils with low bearing capacity (Horn et al., 2007; Allman et al., 2017). Soil compaction is a common consequence of harvesting operations (Ampoorter et al., 2010; Eliasson, 2005; DeArmond et al., 2021) and has [been](#) shown to be detrimental to a number of

35 ecological functions, including soil biota (Beylich et al., 2010), hydrological patterns, and nutrient supply, with potential
36 drawbacks on plant growth and site productivity (Curzon et al., 2022). In addition to soil compaction, machine traffic can also
37 result in deep ruts (Horn et al., 2007; Ala-Ilomäki et al., 2021; Poltorak et al., 2018), which affect site hydrology and increase
38 anaerobic conditions at the rut's base, where air-filled porosity is reduced, leading to minimized soil aeration (Hansson et al.,
39 2019).

40 The risk of causing high degrees of soil compaction and rutting is mainly attributed to soil properties such as initial soil bulk
41 density and texture, as well as the current soil water content (Cambi et al., 2015; Crawford et al., 2021). Moist soils show a
42 higher susceptibility to damage since the internal friction is decreased through water embracing soil particles (Hillel, 1998),
43 reducing the soil bearing capacity and the ability for elastic responses to machine-induced impacts (McNabb et al., 2001).

44 To support forestry management and machine operators, accurate cartographic information on soils with low bearing capacity
45 is essential (Jones and Arp, 2017; Sirén et al., 2019; Campbell et al., 2013). However, existing models that rely on detailed
46 soil maps to retrieve soil mechanical parameters (e.g. Gröll, 2011; Heubaum, 2015) require a high level of input data, and
47 high-resolution soil maps are only available for selected areas, hindering their large-scale application (Vega-Nieva et al.,
48 2009; Kristensen et al., 2019). Therefore, researchers have turned to topographic modelling as a more promising approach
49 (Lidberg et al., 2020; White et al., 2012), as it requires only digital elevation models (DEM), which are increasingly available
50 for most parts of Europe (Hoffmann et al., 2022; Guo et al., 2017). One topographic index that has been extensively studied
51 is the "depth-to-water" (DTW) concept, originally developed and tested at the University of New Brunswick by Meng,
52 Ogilvie, and Arp, as described by Murphy et al. (2007; 2009). The DTW concept calculates flow lines across areas of interest
53 by determining a flow accumulation and selecting lines that originate at a set threshold of accumulated upstream contributing
54 areas. Using a cost function that considers the cell-to-cell slopes, the vertical distances from each cell within a raster to the
55 nearest simulated flow line are ascertained. DTW is well documented (White et al., 2012; e.g. Vega-Nieva et al., 2009; Murphy
56 et al., 2011).

57 Previous research has shown that the DTW index performs relatively well in predicting wet areas in forested formerly
58 glaciated landscapes compared to other indices (Ågren et al., 2014; Larson et al., 2022). Recent studies have explored further
59 developments in moisture prediction by utilizing machine learning algorithms applied to a variety of freely available data and
60 diverse retrieved information, including different topographic indices calculated on DEMs. Ågren et al. (2021) used 28
61 topographic predictor variables in an eXtreme Gradient Boosting model (Chen et al., 2021) to predict soil moisture across the
62 entire Swedish forest landscape at high resolution (2x2 m). Although topographic modelling approaches are widely used, they
63 often fail to adjust to seasonal changes in soil water regimes. Static maps may not adequately represent temporal occurrences
64 of flow lines, wet fields, or water-saturated soils. To address this issue, the DTW concept offers a potential solution, enabling
65 the calculation of different scenarios ranging from 'very dry' or 'frozen' to 'wet' soil conditions. However, selecting the most
66 accurate DTW scenario requires high expertise (Leach et al., 2017: 5434; Lidberg et al., 2020), and mistakes can lead to
67 reduced accuracy and result in potential soil damages that could be avoided.

68 Therefore, we believe that the next crucial step in soil moisture modelling is to incorporate a temporal component that enables
69 the prediction of rasters for any given time and area. One approach to achieve this was designed by Schönauer et al. (2022),
70 who developed a spatiotemporal prediction model. Dynamic satellite-based retrievals of soil moisture with coarse spatial
71 resolution (Soil Moisture Active Passive Mission) were combined with high-resolution but static topographic maps. This
72 resulted in improved performance in predicting moisture values across time-series conducted on sites in Finland, Germany,

73 and Poland. The incorporation of a dynamic component into the prediction model enabled reflection of the current overall
74 moisture conditions on the study sites. This allowed to calculate daily prediction grids that could support forestry practice and
75 enable the guidance of machine operators on sites to avoid traffic on wet areas susceptible to damages. However, a validation
76 of predicting rut depth by models of this kind has not been facilitated yet.

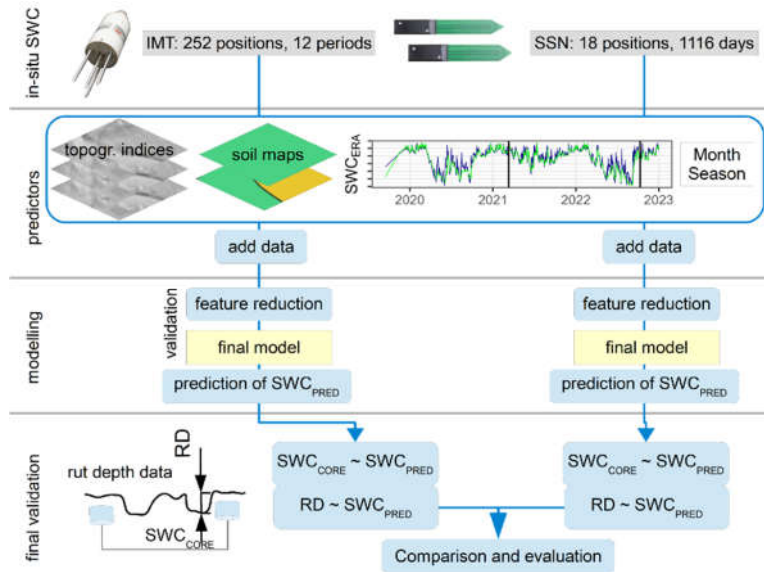
77 The effectiveness of soil moisture modelling, whether based on static or dynamic independent variables, is ultimately
78 constrained by the quality of the dependent variable, which in this case is in-situ soil moisture. Manual measurements of soil
79 moisture have been conducted in numerous studies using different devices, such as hand-held time-domain reflectometry
80 sensors (Kemppinen et al., 2018; Uusitalo et al., 2019) or impedance measuring techniques (e.g. Schönauer et al., 2021b).
81 Despite the potential inaccuracies associated with these techniques (Walker et al., 2004; Francesca et al., 2010), they offer
82 significant advantages in terms of flexibility, scalability, low investment costs, and minimal maintenance. Another option is
83 the use of continuously measuring sensor networks (e.g. Oliveira et al., 2021), which can provide relatively reliable
84 measurements but with limited spatial coverage due to the high costs of installation and maintenance.

85 In this study, we built upon the approach developed by Schönauer et al. (2022) by incorporating additional data sources,
86 including additional topographic indices, soil maps, and soil moisture retrievals from ERA5-Land for two soil depths. The
87 study also used two types of data sources for soil moisture measurements: manual measurements using a handheld moisture
88 meter, and data from two continuously measuring sensor networks. We argue that manual measurements are simpler and can
89 be applied to larger areas, while sensor networks are more expensive and limited to chosen positions.

90 The study had two main objectives: 1. to train soil moisture models using the two individual data sets (manual measurements
91 and sensor networks) and evaluate their prediction performance, and 2. to select the best combination of predictor variables
92 (e.g. topographic indices, ERA5-Land values) using a repeated cross-validation approach and compare the best models with
93 rut depth data obtained during four trials using a forwarder.

94 **2 Material and Methods**

95 To model soil water content (SWC), random forest models were trained using two separate datasets: manual in-situ
96 measurements using an impedance measuring technique (IMT) and continuously measuring soil sensor networks (SSN). To
97 both datasets we added predictor variables derived from topographic indices (e.g. depth-to-water, topographic wetness index),
98 soil maps, SWC estimates from the ERA5-Land campaign (SWC_{ERA}), and numerical values for date (month and season). We
99 performed cross-validation and reduced features stepwise to choose the best-performing model. Subsequently, the two final
100 models (for IMT and SSN) were used to predict SWC for the positions and dates of different field trials with a forwarder.
101 During ~~these~~ field trials, rut depth data was captured, and compared to the predictions from the final SWC-models (Figure
102 1).



103

Figure 1: Soil water content (SWC, [%]) was predicted using models trained on two datasets: in-situ measurements (IMT) and soil sensor networks (SSN). Input variables included topographic indices, soil type data, SWC estimates from ERA5-Land (SWC_{ERA}), and date values. Through cross-validation, we selected the final models, used to predict SWC_{PRED} for various positions and dates during trials with a forwarder. Model estimates were compared with in-situ SWC_{CORE} and rut depth (RD, [cm]).

104 **2.1 Study sites**

105 The data acquisition of volumetric SWC [%] and the trials with a forwarder were conducted in two forest stands located near
 106 the city of Arnsberg in North Rhine-Westphalia (Figure 2). The forest stands were situated at an altitude of approximately
 107 250 m on common soil types such as Cambisol and Stagnosol on Claystone and Sandstone from Devon and Carbon (Table
 108 1).

Table 1. Characteristics of the study sites, where soil water content was captured and field trials with a forwarder were performed.

Site	Coordinates in WGS84		Dominant soil types	Humus form	Slope [%]	Canopy
	x	y				
A	8.039	51.406	Cambisol - Stagnosol	Mesomull	15-30	<i>Fagus sylvatica</i> , <i>Quercus spp.</i> , <i>Pinus sylvestris</i>
B	8.024	51.473	Stagnosol	Mull	1-7	<i>Fagus sylvatica</i>

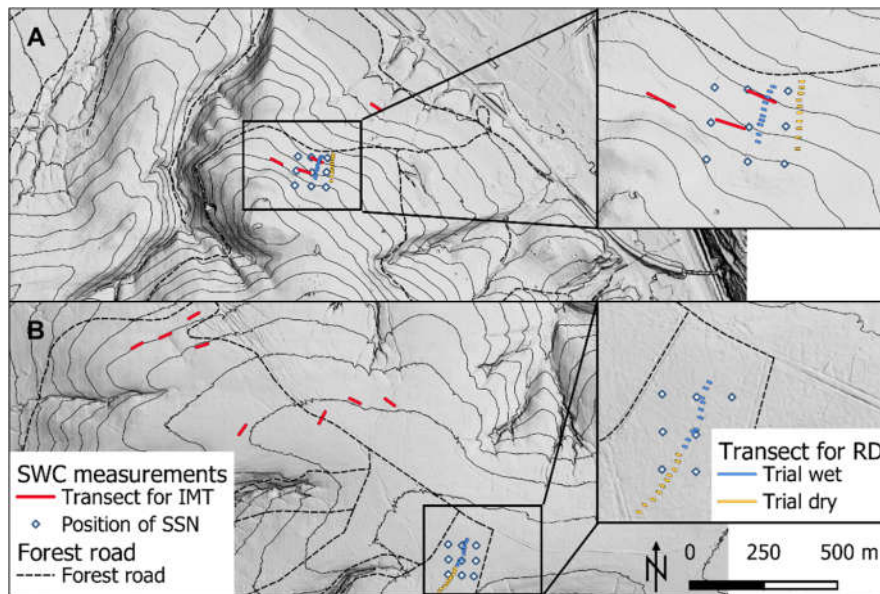


Figure 2: The map indicates the locations of two experimental areas on a hill-shaded digital elevation model with 10 m contour lines; Site A (A, coordinates x, y in WGS84: 8.039, 51.406) and Site B (B, coordinates: 8.024, 51.473), which were used for collecting time-series data on soil water content (SWC). SWC was measured using a handheld soil moisture meter (impedance measuring technique, IMT) along transects (red lines), each containing 21 measuring positions (2 m spacing). In addition, a soil sensor network (SSN) was used to continuously capture SWC at 18 positions (white rhombus). The map also indicates the locations of 40 transects (in crop-outs) used for measuring rut depth (RD) during relatively wet conditions (Trial_{WET}, blue lines) and drier conditions (Trial_{DRY}, orange lines).

109

110 2.2 Soil moisture models

111 2.2.1 In-situ soil moisture

112 Two sets of in-situ data of soil moisture were used: 1. Manual measurements of SWC were performed using a HH2 Moisture
 113 Meter (Delta-T Devices Ltd, England), which applies Impedance Measuring Technique (i.e. ‘IMT’) (Eijkelpamp Agrisearch
 114 Equipment, 2013). 2. Data from a continuously measuring Soil Sensor Network (i.e. ‘SSN’).

115 The IMT data used for this study were previously used for the validation by Schönauer et al. (2022) and consisted of 12
 116 measuring transects. The transects were placed in various positions in broadleaved forests, known to be temporarily wet or
 117 sensitive for machine traffic, with each transect having a length of 40 m. SWC was measured with a spacing of 2 m along the
 118 transects. To measure SWC, measuring rods of 60 mm length were vertically inserted into the soil after removing the humus
 119 layer. The measurements were taken almost monthly between September 2019 and October 2020 (Figure 3B). The IMT data
 120 consisted of 2,184 observations. Overall, this dataset offers a relatively high level of spatial granularity, with 252 measuring
 121 positions. However, the temporal resolution of the data is relatively low, with only monthly measuring campaigns conducted.

122 The SSN was launched in December 2019 and its data was obtained from continuously measuring SMT100 sensors
 123 (TRUEBNER GmbH, Germany), placed on two sites, each having 9 positions with a spacing of 50x50 m. At each position,
 124 two sensors were placed at a depth of 10 cm in the mineral soil, with a temporal resolution of 15 minutes. The data from these
 125 sensors were averaged for each position and each of the 1,116 days captured (data until 2022-12-31 was included), resulting
 126 in a total of 16,351 observations after omitting all missing values. While this data set provides a high level of temporal
 127 granularity, it suffers from a low level of spatial granularity due to the limited number of positions sampled.

128 To enable the incorporation of seasonal effects in the modelling approaches, we transformed the date of each measurement

129 into numeric vectors, resulting in the variables Month and Season. The coding used for Season was as follows: 1 for March,
130 April, and May; 2 for June, July, and August; 3 for September, October, and November; and 4 for December, January, and
131 February.

132 To enable the creation of spatiotemporal data, the positions of all measuring locations were captured using post-processed
133 signals from a GNSS device (Trimble R2 RTK Rover, Trimble, Colorado, USA). This data was then fused with a range of
134 topographic indices. To achieve this, values of several topographic indices were extracted at each measuring position of IMT
135 and SSN.

136 **2.2.2 Topographic indices**

137 For calculating topographic indices, we used a freely available digital elevation model (DEM), as provided by the
138 Bezirksregierung Köln (2020). The resolution of this model was 1x1 m, with a vertical accuracy of ± 0.2 m. Using the free
139 programming language R (version 4.0.2, R Core Team, 2023) and RStudio (version 2022.07.2, Posit PBC, Massachusetts,
140 USA), along with the package "rgrass" (Bivand, 2021) to utilize GRASS GIS (Awaida and Westervelt, 2020) commands in
141 the R interface, the command 'r.hydrodem' was used to 'remove all sinks' (Flags: -a) from the DEM. Thereafter, we calculated
142 depth-to-water (DTW) maps. To generate these maps, we followed the script by Schönauer and Maack (2021) and used flow
143 initiation areas (FIA) of the following sizes 0.25 ha (DTW025), 1.00 ha (DTW1), and 4.00 ha (DTW4), which account for
144 different overall soil moisture conditions. A smaller FIA results in a DTW map for wetter conditions, as the network of
145 simulated flow lines expands, while a larger FIA represents drier conditions. For further details, refer to Murphy et al. (2009;
146 2011).

147 The Topographic Wetness Index (TWI) represents the tendency for water to accumulate at any point in the catchment (Quinn
148 et al., 1991), while the stream power index (SPI) represents the power of water flow at any point in the catchment and the
149 gravitational forces that move water downslope (Moore et al., 1991). To compute TWI, we used the 'r.watershed' command
150 in GRASS GIS, as conceived by Sørensen and Seibert (2007). TWI was calculated as $\ln(\alpha/\tan(\beta))$, where α is the cumulative
151 upslope area draining through a point per unit contour length, and $\tan(\beta)$ is the local slope angle. SPI was calculated as $\alpha * \tan(\beta)$ (Moore et al., 1991). Flow Accumulation, representing the absolute amount of overland flow passing through each cell
153 was also included as a variable. TWI, SPI, and Flow Accumulation were calculated on an aggregated DEM with a spatial
154 resolution of 15x15 m. This resolution has been shown to exhibit a stronger correlation with SWC, and can be assumed to be
155 more robust (Ågren et al., 2014), as observed in prior work where resolutions ranging from 1 to 20 m were tested (data not
156 shown). In addition, we calculated the variable Slope [$^{\circ}$] using the R-package 'raster' (Hijmans, 2020).

157 **2.2.3 Soil maps**

158 Soil maps of North Rhine-Westphalia were originally generated at a scale of 1:5,000 from forest site surveys. We included
159 soil type information (Soil05) for the analysis. While these maps are not available across the entire region of North Rhine-
160 Westphalia, they were provided for the study sites by the Geological Survey of North Rhine-Westphalia. By contrast, soil
161 maps with a scale of 1:50,000 are available for the entirety of North Rhine-Westphalia (Soil50).

162 **2.2.4 Temporal soil water content from ERA5-Land**

163 ERA5-Land is a global reanalysis dataset providing hourly estimates of meteorological variables at a spatial resolution of 9x9

164 km, including soil moisture [$\text{m}^3 \text{m}^{-3}$] at the top soil layer (0-7 cm, 'layer 1' (L1)) and at a depth of 7-28 cm ('layer 2' (L2)).
165 ERA5-Land data is retrieved by assimilating satellite and atmospheric forcing (Muñoz-Sabater et al., 2021). ~~It provides a~~
166 ~~reliable representation of soil moisture values and variations across the majority of global regions, making it applicable for~~
167 ~~various geophysical applications (Lal et al., 2022).~~

168 We opted for ERA5-Land retrievals to address the temporal component of SWC, as this dataset offers a dependable
169 representation of soil moisture values and their variations across global regions, rendering it suitable for various geophysical
170 applications (Lal et al., 2022). Additionally, this decision is grounded on two key assumptions: 1. The spatial variability of
171 SWC is relatively low compared to its temporal variability. 2. The spatial extent of our measurement locations is small and
172 cannot be adequately captured by satellite-based Earth observation data. Even Sentinel-1, a mission within the Copernicus
173 Programme by the European Space Agency renowned for supporting high-resolution (1x1 km) surface soil moisture product
174 generation (Peng et al., 2021), would have limited utility in providing spatial information for our study sites. For instance, the
175 maximum distance between rut depth transects (Section 2.3.2) was 200 m. Furthermore, since Sentinel-1 focuses on surface
176 soil moisture using the C-Band, we assume that ERA5-Land's soil moisture estimates for deeper layers might offer a better
177 fit for our data, as suggested by similar findings presented by Fjeld et al. (2024).

178 We utilized the API provided by CDS (Copernicus Climate Change Service, 2019) and the R-package 'ecmwf' (Koen Hufkens
179 et al., 2019) to download daily grids (at 14:00 UTC) of layer 1 and 2. The downloaded data covered both the whole time span
180 of our data and the two measuring sites. Both sites were situated in one 9x9 km raster cell of the ERA5-Land. The land cover
181 for this cell was derived from Bezirksregierung Köln (2023), showing that open land (e.g. grassland, crops) dominated with
182 52% of the total cover, whereas forests occurred on approximately 31% of the cell size, followed by 12% coverage from
183 infrastructure, 3% loose material, and 2% water bodies.

184 After downloading the data, we stacked the daily grids and extracted the corresponding values at each measuring position,
185 giving $\text{SWC}_{\text{ERAL1}}$ and $\text{SWC}_{\text{ERAL2}}$.

186 All data, the topographic information, soil types, numerical values of date and the dynamic variables from ERA5-Land were
187 merged with in-situ data, either IMT or SSN.

188 2.2.5 Modelling

189 The modelling approach described here was applied separately for both data sets, IMT and SSN (and for both datasets
190 combined). ~~(the main outputs when both datasets were combined can be seen in Figure A1).~~

191 Initially, we fitted a linear model with SWC as the dependent variable and $\text{SWC}_{\text{ERAL1}}$, $\text{SWC}_{\text{ERAL2}}$, Month, Season, DTW025,
192 DTW1, DTW2, DTW4, Slope, TWI, SPI, Accumulation, Soil05, and Soil50 as the independent variables. We then used this
193 linear model to check the data for autocorrelations and subsequently eliminated variables with a variance inflation factor > 10
194 through an iterative process, reducing one variable at a time. Also, the feature selection according to the Boruta algorithm
195 (package 'Boruta', Kursa and Rudnicki, 2010) was applied.

196 We then trained random forest models (Breiman, 2001), repeatedly reported as efficient in predicting complex data (Cavalli
197 et al., 2023; Carranza et al., 2021; Kemppinen et al., 2018), using the 'ranger' package (Wright and Ziegler, 2017) with a 10-
198 fold cross-validation with 5 repetitions. For each of the 50 models in the validation of one configuration, we noted the mean
199 of Kendall's coefficient of correlation τ (since different sample sizes occurred) of the random forests and the representative
200 standard deviation. In addition, the least important variable according to impurity and its frequency within the 50 validation

201 sets were traced. The variable noted most frequently as least important was then removed, and a new cross-validation was
202 performed on $SWC \sim (n-1)$ variables, with n being the number of predictors in the model trained previously. This process was
203 repeated until only one predictor variable remained.

204 To avoid temporal autocorrelations at the measuring positions, positions IDs were used to select the folds of the cross
205 validations.

206 **2.2.6 Selection of the final model**

207 To select the final random forest model for each data partition, we examined the maximum τ values obtained and multiplied
208 them by 0.99 (according to Hauglin et al. (2021)). This was done to penalize the use of an unnecessarily high number of
209 predictor variables. We selected the model with the least number of predictor variables within this 1%-range as the final
210 model. The final models (built on IMT and SSN data) were then used to predict rasters of SWC_{PRED} , which were visually
211 evaluated. Subsequently, the outputs of the final models were compared to rut depths and SWC at the machine operating
212 trails.

213 **2.3 Data from field trials with a forwarder**

214 **2.3.1 Rut depth (RD)**

215 During the field trials conducted in two forest stands at two seasons, a fully loaded forwarder (John Deere 1210G, 8-Wheel
216 model, total mass of 28 Mg (18 Mg machine weight + 10 Mg loading)) was used. The first trial was conducted on section 1
217 of an existing machine operating trail on 2021-03-11, during generally wet conditions (Trial_{WET}). The second trial was
218 conducted on subsequent section 2 of the same machine trail on 2022-10-11, during drier conditions (Trial_{DRY}) (Figure 2,
219 Site [BA](#)), or in close proximity of section 1 (Site [BA](#)), as there the machine trail was not long enough for both sections.

220 The four trials were positioned near the sensors of the SSN (Figure 2) and, in the case of Site A, near the IMT measuring
221 transects. On Site B, the IMT transects were at a distance of 530 m to 1300 m. Moreover, there is a temporal lag between the
222 IMT measuring campaigns and the field trials (Figure 3). This discrepancy stems from the IMT data being collected as part
223 of a separate research project.

224 The 8-wheel machine trafficked section 1 and 2 of both operating trails, and made four passes. Before the first machine pass,
225 the initial surface was captured along 10 perpendicular transects on each of the four sections. These 4 m wide transects were
226 placed and marked permanently with inserted wooden pegs. The same pegs were used to position the beam, which served as
227 the reference height to measure profiles along each transect. Into this beam, metric scales were inserted with a spacing of 10
228 cm in between, to note the distance between the surface and the beam to the nearest cm. These measured distances (D_0 , [cm])
229 describe the surface along the transect on already existing machine operating trails, prior to the trial conducted in this study.

230 The same procedure was repeated after the fourth consecutive machine passes, giving D_4 [cm].

231 Next, the differences between D_0 and D_4 were calculated at each of the 41 measurements (10 cm spacing over 4 m) along a
232 transect. The maximum value of these differences, measured at the left or right machine track, was used to determine rut depth
233 (RD, [cm]). We used average values of both tracks to prevent pseudo replicates, since intraclass correlation coefficient was
234 high (0.83), when left and right tracks were integrated separately. Moreover, mean and maximum values of rut depth were
235 highly correlated (adj. $R^2 = 0.96$).

236 Rut depth (Four of the 40 transects for measuring RD, [cm]) was measured during four trials with a forwarder, covering 10

237 transects for each trial. This provided us with the potential for 40 measurements, but unfortunately, 4 of them were not
238 ascertainable as the forwarder destroyed the wooden pegs that positioned the reference beam. In Trial_{WET}, conducted in March
239 2021, SWC_{ERA1} and SWC_{ERA2} showed a soil moisture level of 39%. At Site A, the measured RD was 10.3±1.9 cm, while
240 at Site B, the RD was 12.7±5.5 cm, with the highest value of RD recorded after 4 passes, with a depth of 21.5 cm. In Trial_{DRY},
241 conducted in October 2022, the soil water content from ERA5-Land was 32%. At Site A, the measured RD was 3.5±1.7 cm,
242 and at Site B, the RD was 4.3±1.2 cm. Comparisons of RD with DTW and TWI are given in Figure C1.

244 2.3.2 Soil water content at the rut depth transects (SWC_{CORE})

245 Volumetric soil moisture content was captured outside the 1st, 4th, 7th and 10th transect of each section, with a distance of 1 m
246 to the left and right track, at a depth of 10-15 cm. This water content was determined using 100 cm³ cores taken with an
247 undisturbed core sampler, with three replicates at each measurement. SWC_{CORE} was calculated according to equation (1):

$$248 \text{SWC}_{\text{CORE}}[\%] = \frac{M2 - M1}{M1} * 100 \quad (1),$$

249 with M2 being the fresh mass of the soil taken with undisturbed cores and M1 being the mass after drying the samples in oven
250 with 105 °C, until mass constancy was reached.

251 Measurements of RD and SWC_{CORE} were georeferenced using the GNSS devise and complemented with all the predictor
252 variables, as described above.

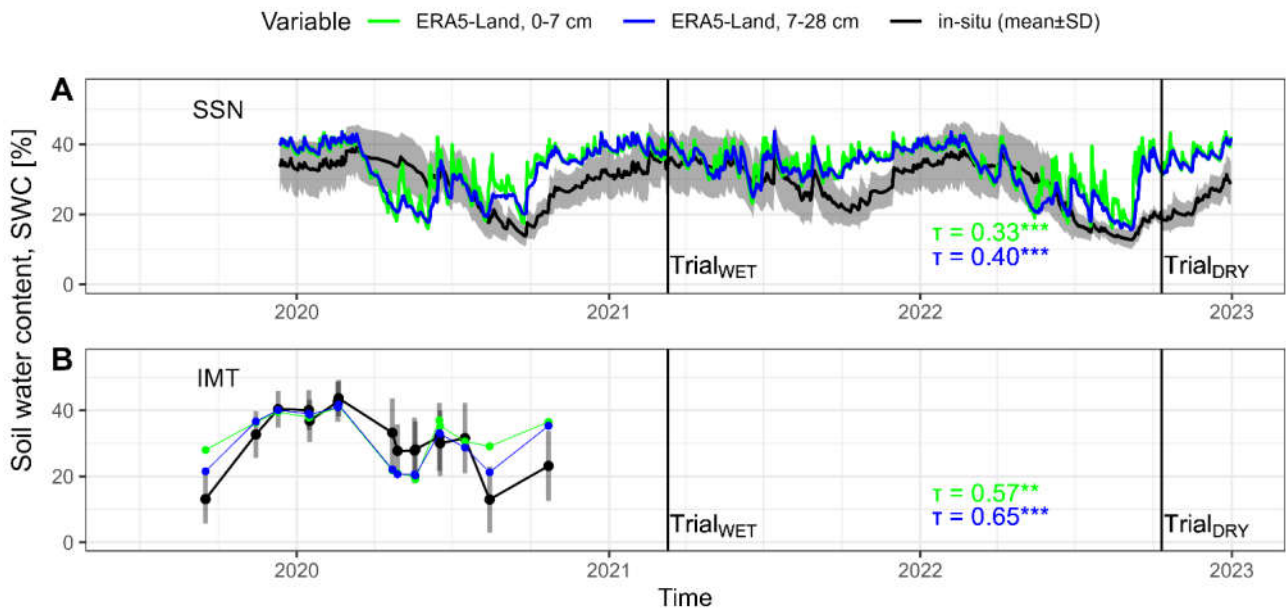
252 2.4 Comparisons between model predictions and RD or SWC_{CORE}

253 For the ‘testing on rut depth data’ (Figure 1), values of SWC_{PRED} were compared to RD or soil water content, captured through
254 undisturbed cores along the transects, SWC_{CORE}. The predictor variables from the rut depth dataset were used to predict
255 SWC_{PRED} by means of the final random forest models created in the soil moisture modelling. Since the goodness-of-fit
256 between in-situ values of RD or SWC_{CORE} and SWC_{PRED} was to some degree sensitive to the seed set during modelling, we
257 repeated the predictions ten times and used average values to receive robust estimates of SWC_{PRED}. To test the correlations
258 between paired samples of SWC_{CORE} or RD and SWC_{PRED}, Kendall's rank correlation was used. We illustrated the
259 corresponding p-values as follows: ‘***’ for p<0.001, ‘**’ for 0.001-0.01, ‘*’ for 0.01-0.05, (‘*’) for 0.05-0.10 and ‘ns’ for p-
260 values being higher than 0.10. [Root mean squared error \(RMSE\) and mean squared error \(MSE\) were calculated according to](#)
261 [Hamner and Frasco \(2018\)](#). Values are given as mean±standard deviation.

262 3 Results

263 3.1 Soil water content

264 The mean value of SWC, measured using a handheld moisture meter (IMT), varied between 13.0±10.0% in August 2020 and
265 43.2±5.95% in February 2020 (Figure 3). Daily mean values obtained from soil sensor networks (SSN) were similar to those
266 obtained from IMT, ranging from 13.8±2.90% in September 2020 to 39.1±6.66% in March 2020, in the period that
267 corresponds to the one covered by IMT. The driest conditions were observed in September 2022, with a daily mean SWC of
268 12.7±2.55%. Overall, the results suggest that IMT and SSN provide comparable estimates of SWC, with the latter providing
269 higher temporal resolution at a low spatial granularity.



270
271

Figure 3: Time series of soil water content (SWC) measured using a soil sensor network SSN (A) with 18 measuring positions on two sites and manual measurements, using impedance measuring technique IMT (B) conducted on 252 positions (black lines/points show daily mean values, grey shading/bars show standard deviation for each day). SWC retrievals from ERA5-Land are shown as a blue line/point (0-7 cm vertical resolution, as available from Copernicus Climate Change Service (2019)) and a green line/point (7-28 cm vertical resolution). The goodness-of-fit between daily means of measured SWC and ERA5-Land retrievals is reported using Kendall's rank correlation coefficient (τ). Vertical lines indicate the dates of the trials when a forwarder conducted four passes at existing machine operating trials.

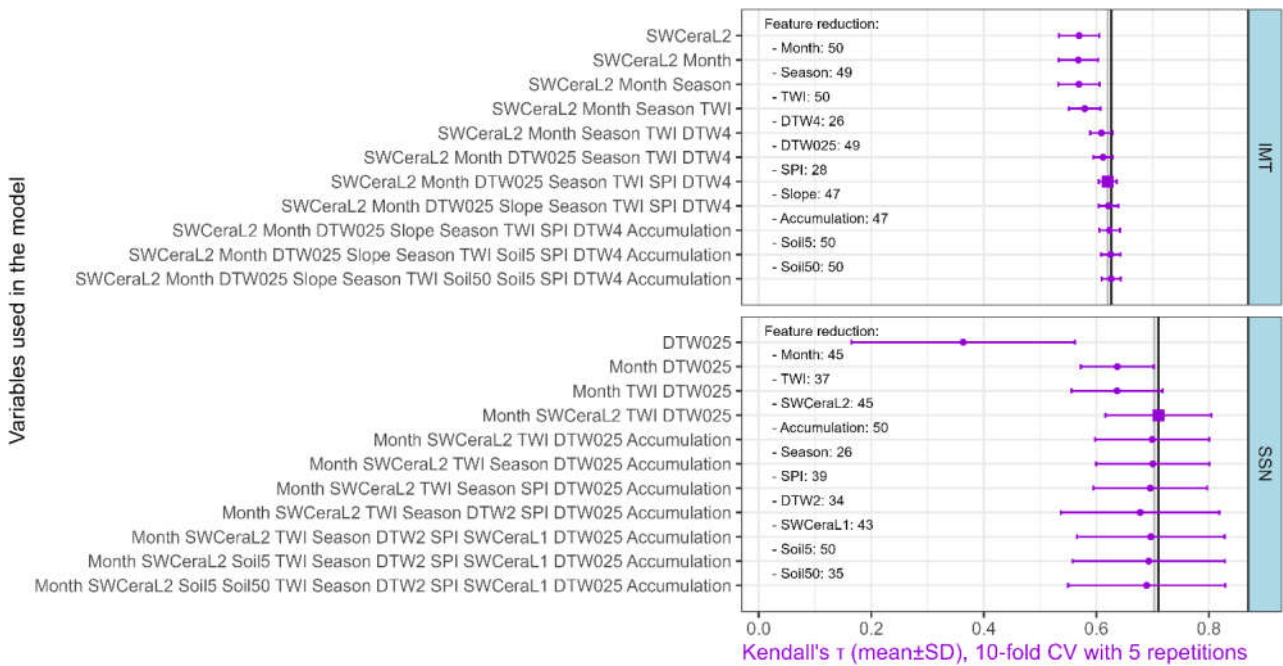
272 **3.2 Soil moisture models**

273 The positions IDs were used to select the 10 folds for cross-validation. However, the dataset SSN had only 18 measuring
274 positions (where SWC was measured on 1116 days), resulting in relatively high deviations of Kendall's τ of the random
275 forests. The most important feature for this dataset was given by DTW025, although the resulting quality was low, with τ of
276 0.363 ± 0.198 . By adding the temporal component Month, the τ improved to 0.637 ± 0.065 , which had the lowest standard
277 deviation for the repeated folds. The final model for this dataset included the temporal variables Month and SWC_{ERA5L2} , as
278 well as the topographic predictor variables TWI and DTW025 (Figure 4). The resulting τ was 0.710 ± 0.095 , revealed through
279 the cross-validation.

280 For the IMT partition, which had a low temporal but high spatial resolution, the most important feature was the temporal
281 information SWC_{ERA5L2} , leading to a τ of 0.569 ± 0.036 . The final model had an τ of 0.620 ± 0.016 , including the predictor
282 variables SWC_{ERA5L2} , Month, Season, and DTW025, TWI, SPI and DTW4.

283 [The main outputs when both datasets were combined can be seen in Figure A1.](#)

284

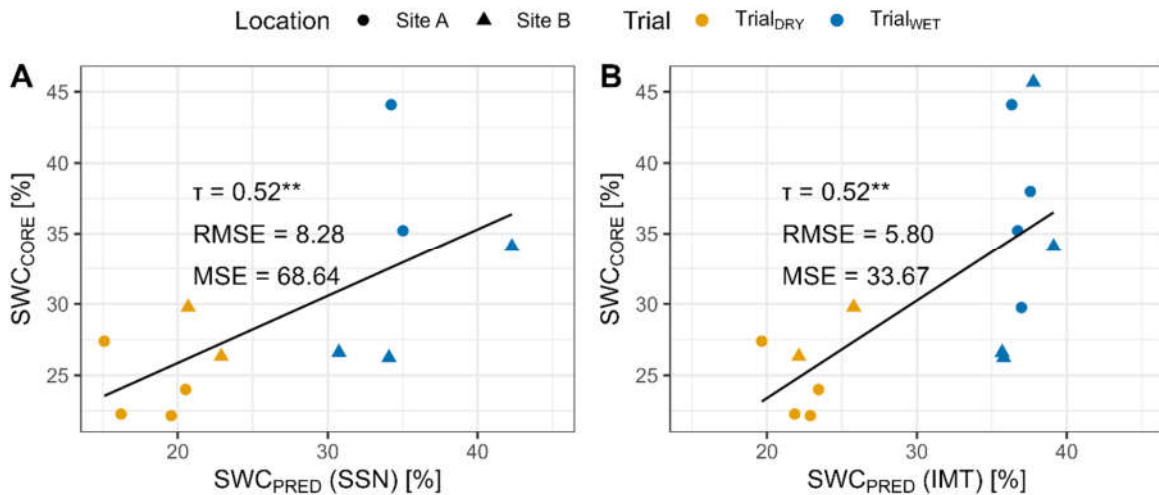


285

Figure 4: Soil water content (SWC) was modelled by random forests (RF), and evaluated by a repeated 10-fold cross validation (CV). Mean values and standard deviation of resulting values of the Kendall rank correlation coefficient τ during the CV are shown. A stepwise elimination of the least important variable was performed, and the frequency of this variable over all models is provided (“Feature reduction”). The vertical lines indicate the maximum value of τ (black) and the 99% of the maximum (grey), to select final models (squares). Variables used are described in section 2.

286 3.2.1 Comparisons of SWC_{CORE} with SWC_{PRED}

287 The final random forest models of both, the IMT and SSN dataset, were used to calculate SWC_{PRED} on the predictor variables
 288 of the rut depth data, including SWC_{CORE} measured at the outside of a subsample of the measuring tracks by undisturbed
 289 cores. The comparison between SWC_{CORE} and SWC_{PRED} values predicted by the final random forest models of both datasets
 290 (SSN and IMT), revealed a significant association (Figure 5).



291

Figure 5: Soil water content was measured during two trials with a forwarder along a machine operating trail ($n=14$), using 100 cm^3 undisturbed cores (SWC_{CORE}), and compared to values predicted (SWC_{PRED}) by a model trained data from a continuously measuring soil sensor network (SSN, A), or manual measurements with a handheld moisture meter (IMT, B). Correlations were evaluated

using Kendall's τ and significance levels are indicated by *** for $p < 0.001$, ** for 0.001-0.01, * for 0.01-0.05, (*) for 0.05-0.10, and 'ns' for $p > 0.10$.

3.3 Interrelations between rut depth and topographic indices or SWC

Rut depth (RD, [cm]) was measured during four trials with a forwarder, covering 10 transects for each trial. This provided us with the potential for 40 measurements, but unfortunately, 4 of them were not ascertainable as the forwarder destroyed the wooden pegs that positioned the reference beam. In Trial_{WET}, conducted in March 2021, SWC_{ERA L1} and SWC_{ERA L2} showed a soil moisture level of 39%. At Site A, the measured RD was 10.3 ± 1.9 cm, while at Site B, the RD was 12.7 ± 5.5 cm, with the highest value of RD recorded after 4 passes, with a depth of 21.5 cm. In Trial_{DRY}, conducted in October 2022, the soil water content from ERA5-Land was 32%. At Site A, the measured RD was 3.5 ± 1.7 cm, and at Site B, the RD was 4.3 ± 1.2 cm.

3.3.11.1.1 Comparisons of RD with DTW and TWI

Considering the significance of the topographic indices DTW and TWI in the development of the SWC models (Figure 4), we aimed to compare RD with both indices. Notably, RD exhibited a clear correlation with DTW025, the most conservative DTW scenario (Figure 6). TWI also demonstrated a correlation with RD.

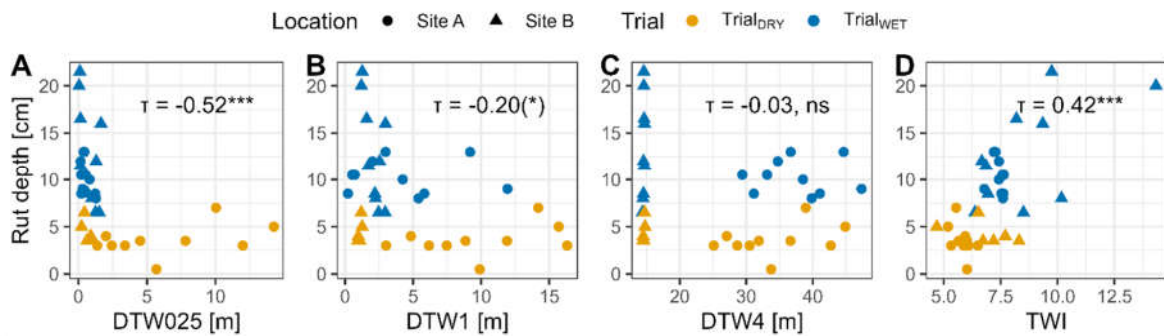


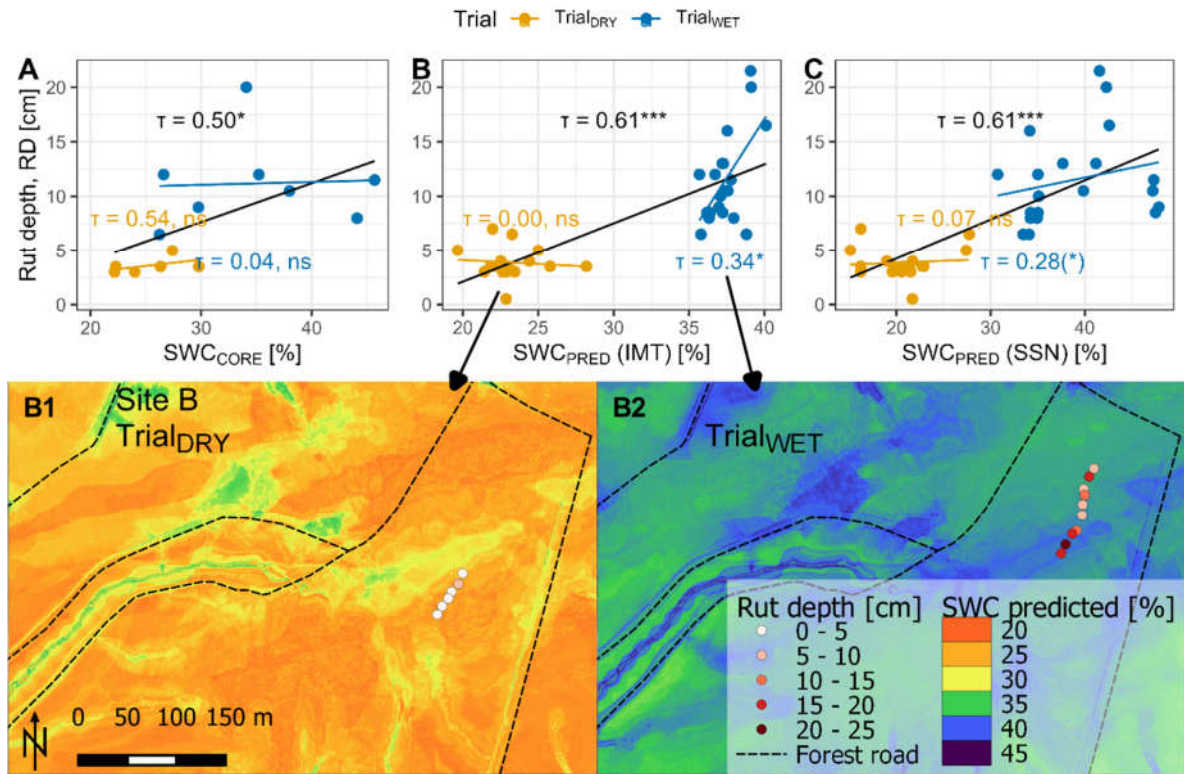
Figure 6. Rut depth (RD) was determined after four passes of a forwarder, driving on two Sites (A and B), during two conditions (Trial_{WET} and Trial_{DRY}). RD was compared to the topographic indices depth to water (DTW), calculated with different flow initiation areas (0.25 – 4.00 ha), and the topographic wetness index. Correlations were evaluated using Kendall's τ and significance levels are indicated by *** for $p < 0.001$, ** for 0.001-0.01, * for 0.01-0.05, (*) for 0.05-0.10, and 'ns' for $p > 0.10$.

While showing significant correlations, the nature of these static maps does not allow for the representation of current moisture conditions. This limitation was overcome when using the predicted (or observed) values of SWC.

3.3.23.3 Comparisons of RD with SWC_{CORE} and SWC_{PRED}

RD was positively correlated with SWC_{CORE} when both trials with different moisture conditions were included in testing (Figure 6A). However, when each trial was tested separately, no correlation between RD and SWC_{CORE} was observed (Figure B1). Compared to the correlation between RD and SWC_{CORE}, modelling outputs SWC_{PRED} proved to be a better predictor of rut depth, particularly for Trial_{WET}. The final models that were selected for both datasets produced a Kendall's τ of 0.61 (for IMT, Figure 6B, and SSN, Figure 6C), when comparing RD of the four trials with the corresponding SWC_{PRED}. Although the R^2 values for these models were in similar range (0.620 for IMT and 0.549 for SSN), we chose to use Kendall's τ since different sample sizes were involved in the analysis. This was particularly relevant for comparing RD with SWC_{PRED} for each Trial separately. While no correlation could be found for Trial_{DRY}, correlations were found for Trial_{WET}, with Kendall's τ of 0.344

316 ($p=0.037$) and 0.281 ($p=0.090$), for the final models trained on IMT and SSN, respectively (Figure 6B,C). Yet, these
 317 correlations seem to be fragile, as a difference of a few percent of predicted SWC_{PRED} (IMT) is associated with the range of RD
 318 between 6.5 and 21.5 cm. Moreover, when analysing the sites separately, a vague trend between SWC_{PRED} and RD could be
 319 observed, but without showing significant correlations (Figure B1, Figure B2).
 320 Since the final model trained on IMT data performed slightly better in Trial_{WET} compared to the model trained on SSN data
 321 (Figure 6), we chose the IMT model for the generation of prediction rasters for the days of interest (Figure 6B1, B2).
 322



323
 324 Figure 6: Rut depth (RD) was determined after four passes of a forwarder, driving on two Sites, during two conditions (WET and
 325 DRY). RD was compared to SWC values, determined for undisturbed soil cores (A) and SWC values predicted by a random forest
 326 model trained on manually obtained IMT measurements (B, see Figure 1) and predicted by a model trained data from a continuously
 327 measuring soil sensor network (SSN, C). Correlations were evaluated using Kendall's τ . The correlation of all values is given in
 328 black, blue and yellow show the Trials during wet and dry conditions. Significance levels are indicated by *** for $p < 0.001$, **
 329 for $0.001-0.01$, * for $0.01-0.05$, (*) for $0.05-0.10$, and 'ns' for $p > 0.10$. The model based on IMT data (B) was used to calculate
 330 prediction rasters for the days of the field trials (B1, B2).

324 4 Discussion

325 4.1 Importance of predictive systems

326 Wet soils are prone to soil disturbances like the formation of deep ruts (Poltorak et al., 2018; McNabb et al., 2001), since
 327 water implies a reduction of particle-to-particle bondings within the soil (Hillel, 1998), decreasing the resistance to external
 328 forces. Consequently, accurate predictions of soil water content (SWC) and soil trafficability is essential for sustainable forest
 329 management and cost-effective, environmentally friendly harvesting operations (Vega-Nieva et al., 2009; Mattila and Tokola,
 330 2019; Picchio et al., 2020; White et al., 2012; Murphy et al., 2007; Mohtashami et al., 2017; Uusitalo et al., 2020). Topographic

331 modelling requires minimal input and the temporal variables used in the final model presented here, are freely available
332 (Copernicus Climate Change Service, 2019). A spatiotemporal model predicting SWC could improve the guidance of machine
333 operators in forest sites during harvesting operations, for example by the effective positioning of brush mats (Labelle et al.,
334 2019; Labelle and Jaeger, 2018). Practical use of static, topographic maps has already been observed in Canada and
335 Scandinavian countries (Ring et al., 2022). By incorporating a temporal aspect, the accuracy of these tools could be further
336 improved. This has the potential to enhance sustainable forest management by protecting soil and mitigating harmful sediment
337 transport (Ågren et al., 2015; Lidberg et al., 2020; Kuglerová et al., 2017; White et al., 2012).

338 **4.2 Comparison to previous work on predictions of SWC**

339 Since soil moisture predictions are crucial for a variety of forestry aspects, several publications have focused on this topic
340 before. For example, Lidberg et al. (2020) predicted soil moisture classes using spatial models built on topographic indices,
341 correctly classifying 73% of wet areas in a Swedish case study. Ågren et al. (2014) reported accurate predictions for 87-92%
342 of observations by comparing soil moisture classes to DTW maps. Larson et al. (2022) used data from the Krycklan catchment
343 and found an accuracy of 84% when comparing moisture classes to the recently developed 'SLU soil moisture map' (Ågren
344 et al., 2021). However, these validations were based on static topographic maps. One attempt to make such static maps
345 dynamic was realized within the DTW concept, which can be customized to calculate various scenarios to adjust to general
346 moisture conditions (e.g., flow initiation areas of 0.25, 1, and 4 ha for wet, moist, and dry conditions, respectively), but
347 selecting the most appropriate scenario during practical use can be a challenging task that requires significant expertise (White
348 et al., 2012; Lidberg et al., 2020; Leach et al., 2017: 5432). To overcome this challenge, we aimed for improvement of soil
349 moisture prediction and refined the spatiotemporal approach conceived by Schönauer et al. (2022). During cross-validation
350 of IMT data from sites in Finland, Poland, and parts of the data used in this work, they reported an R^2 of 0.80. The models for
351 the present study showed an R^2 of 0.759 ± 0.136 (SSN) or 0.636 ± 0.040 (IMT), corresponding to Kendall's τ of 0.710 ± 0.095
352 or 0.620 ± 0.016 , respectively. Although this may not seem like an improvement, it should be noted that the data from German
353 sites had less explanatory power of topography for predicting SWC. For example, DTW4 alone explained SWC to a very
354 limited extent ($R^2 = 0.037^{***}$).

355 **4.3 Prediction of rutting**

356 Besides the comparisons of SWC with DTW maps, various studies have also investigated the capability of topographic indices
357 in predicting rutting – with conflicting outcomes. For example, Vega-Nieva et al. (2009) found that 65% of ruts deeper than
358 25 cm were located in areas with a DTW value of less than 1 m, and 93% of these ruts occurred in areas with DTW values
359 less than 10 m. Similarly, Heppelmann et al. (2022) observed a high frequency of severe rut depth in areas with DTW values
360 less than 1 m in Norway. However, Mohtashami et al. (2017) did not find evidence of such patterns in a field trial where the
361 inclusion of DTW values did not improve the accuracy of a linear model to describe the extents and degrees of rut depth on
362 machine operating trails. In agreement, Schönauer et al. (2021a) found no evidence that DTW or TWI could predict rut depth
363 in a field trial conducted in a temperate broadleaved stand. In this study, we found a significant correlation between RD and
364 DTW025 with a Kendall's correlation coefficient (τ) of -0.52^{***} . Yet, this correlation has to be seen with caution: It is mainly
365 driven by differing ranges of RD between the two Trials, as can be seen in A. We observed that the temporal adjustments of
366 the model based on current moisture conditions improved predictions of rutting by up-to-date SWC predictions, leading to a

367 τ of 0.61*** (Figure 6B,C). While a strong association between RD and predicted values of SWC was observed, the influence
368 of differences between the trials is evident. However, the ranges of RD for each trial were consistent with the SWC predictions.
369 In Trial_{WET}, a significant correlation between RD and SWC_{PRED} was observed (Figure 6B). We hypothesize that the wetter
370 conditions during this trial, which lead to soil destabilization (Hillel, 1998; McNabb et al., 2001), enhanced the predictive
371 power of topographic indices representing soil water distributions. For instance, DTW025 overlapped with surface water in
372 depressions, as observed in the field campaigns for Trial_{WET}.
373 In contrast, during Trial_{DRY}, no correlation was found between RD and SWC_{PRED}. SWC along the measuring sections was
374 likely below the threshold for soils to become susceptible to deformation. For example, Poltorak et al. (2018) stated that ruts
375 only occurred on soils with an SWC above 50%, whereas SWC_{CORE} at Trial_{DRY} was below 30% (Figure 5).

376 4.4 Description of the model

377 The best-performing model in predicting RD incorporated temporal information from SWC_{ERA2}, Month and Season, as well
378 as spatial information from DTW025, TWI, SPI and DTW4, and was based on data from the manual measurements (IMT).
379 The IMT data was collected in close proximity to the rut depth measurements at Site A (Figure 2), or with a distance of up to
380 1.3 km at Site B. However, the spatial distance between the IMT training data and the rut depth data did not seem to be crucial
381 for the accuracy of predicting rut depth (Figure B2, Figure B1), since Kendall's τ between RD and SWC_{PRED} was similar for
382 both sites. Surprisingly, the correlation between in-situ SWC_{CORE}, sampled directly at the machine operating trails, showed a
383 lower explanatory power in predicting RD than SWC_{PRED}. Although an overall association between RD and SWC_{CORE} was
384 confirmed, no correlation could be found when trials were analysed individually.

385 4.4.1 Temporal variaton was higher-more important than spatial variation

386 The lacking association between RD and SWC_{CORE} on individual trials indicates that the temporal variability in soil moisture
387 between the trials was more important in this study than the spatial variability within the relatively small areas where each
388 trial was conducted. The spatial distribution of the rut depth measurements might have been limiting in the present work. The
389 semivariogram indicates the spatial covariation of rut depth and SWC (Figure 7). While the covariation of RD in Site A is
390 indicated to be high within a range of 10 m (RD-transects were at this distance), on Site B during wet conditions, the sill of
391 the semivariogram reaches almost 40 m, which covered a high number of transects. Similarly, excluding soil information in
392 the initial stages of feature reduction suggests homogeneous soil properties on the relatively small study area.

393 Therefore, we have to admit, that the study design was not ideal for assessing the ability to predict rutting with a spatiotemporal
394 model of SWC, and the results have to be considered with caution.

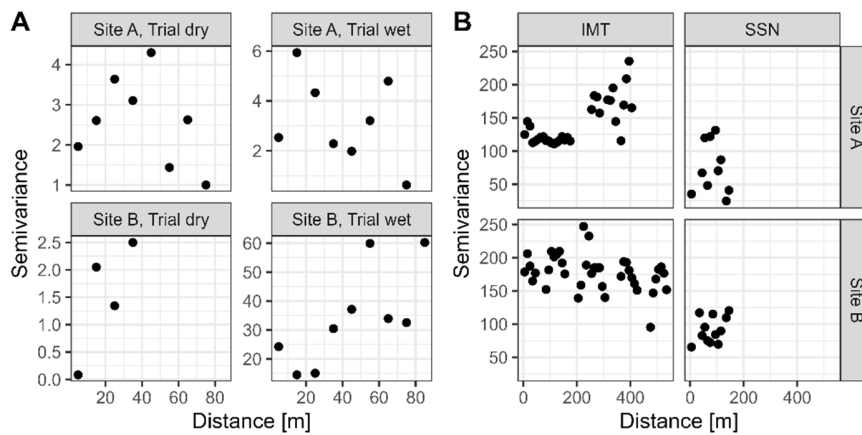


Figure 7. Semivariogram illustrating spatial autocorrelation of (A) rut depth (cm) and (B) soil water content (SWC) across the study area. Rut depth was measured during two moisture conditions, at four machine operating trail sections, allocated on two sites. The measuring transects had a spacing of 10 m. SWC was measured with handheld measuring techniques (IMT), or a soil sensor network (SSN) (Figure 2).

395

396 The spatiotemporal model (IMT), also supports the conclusion that spatial variations were ~~wether-either~~ underrepresented by
 397 the study design (or very low compared to temporal variation by nature) as the temporal feature $SWC_{ERA}L2$ was selected as
 398 most important variable and the difference between the model with one predictor variable vs. the final model was small
 399 (Figure 4).

400 Still, this slight increase in the models' quality allowed for the integration of spatial patterns and resulted in the significant
 401 but vague prediction of RD in Trial_{WET} ($\tau = 0.344^*$, Figure 6). Another indication of the integration of spatial patterns can be
 402 interpreted by the segregation of the temporal range of the IMT data (2019-2020) and the actual Trials (March 2021 and
 403 October 2022, Figure 3), indicating a generalization of spatial and temporal patterns.

404 4.4.2 Most important variables

405 In the final model (IMT), $SWC_{ERA}L2$ has been identified as the most important variable, followed by Month and Season. It is
 406 noteworthy that in the data with broader spatial coverage (i.e. IMT), in contrast to the SSN data, dynamic variables took
 407 precedence over predictor variables. Surprisingly, when modelling SSN data, characterized by high temporal resolution and
 408 low spatial resolution, DTW025 remained the most influential variable. One might have anticipated the opposite, expecting a
 409 topographic index to play a central role in modelling IMT data, and dynamic SWC_{ERA} variables dominating the modelling of
 410 SSN data.

411 We presume that the low spatial variations of SWC in comparison to temporal variations, inadequately represented by the
 412 provided topographic information, may have contributed to this unexpected outcome. Furthermore, the wider spatial coverage
 413 in the IMT data likely resulted in more robust averages of SWC, leading to a stronger correlation with the coarse spatial data
 414 of ERA5-Land (9x9 km). On the contrary, the SSN data, originating from areas with a size of 100x100 m and known for their
 415 temporal wetness, could explain the heightened importance of DTW025. Some sensors might have measured constant water
 416 saturation, thereby inflating the explanatory power of topographic information. These assumptions are speculative, and further
 417 research in this direction is warranted.

418 In the feature reductions of IMT and SSN data (Figure 4), $SWC_{ERA}L2$ (7-28 cm soil depth) dominated over $SWC_{ERA}L1$ (0-7
 419 cm). This aligns with in-situ measurements of SWC by the SSN, conducted at a soil depth of approximately 10 cm (Figure

420 3A). Even for the IMT data, where SWC was measured in the top 6 cm of soil, SWC_{ERA2} yielded a better goodness-of-fit
421 compared to SWC_{ERA1} (Figure 3B). We hypothesize that the prevalence of open lands as the dominant land cover form in
422 the ERA5-Land raster cell (section 2.2.4) contributed to the superior fit of SWC_{ERA2} . Grasslands typically exhibit higher
423 temporal heterogeneity of soil moisture compared to forests (James et al., 2003). This temporal heterogeneity tends to decrease
424 with deeper soil layers (Tromp-van Meerveld and McDonnell, 2006). Therefore, the stronger correlation between SWC_{ERA2}
425 and SWC, as well as its higher importance within the random forests, seems reasonable. The disparity between SWC_{ERA} and
426 in-situ SWC can be attributed to the high transpiration rates in forests, as opposed to grass (Kelliher et al., 1993).

427 **4.5 Further developments**

428 The terrain data was derived from a digital elevation model, which is increasingly available for the entire Europe (Hoffmann
429 et al., 2022), while the dynamic variables are based on data and retrievals from ERA5-Land, which are freely available up to
430 a few days ago. These inputs would allow for automated mapping of current soil water content, which could be made
431 accessible to forestry stakeholders. Recent developments also show a pathway to integrate medium and long range weather
432 forecasts into trafficability predictions, as conceived by the Finnish Meteorological Institute (2023). Both, recent as well as
433 forecasting predictions can lead to improved soil protection, higher efficiency of timber harvesting (Suvinen and Saarilahti,
434 2006), and a new stage of sustainable forest management (Campbell et al., 2013; D'Acqui et al., 2020; Uusitalo et al., 2019;
435 Jones and Arp, 2019). However, it should be noted that the in-situ data of SWC originated from manual measurements, and
436 it was relatively labor-intensive to gather this amount of data. There is potential to reach appropriate accuracy even with a
437 reduced dataset - further investigation would be necessary to determine the essential input data criteria. The alternative to
438 manual measurements is given by sensor networks, which led to comparable results, but such sensor networks are expensive
439 to establish and maintain. Nonetheless, initiatives of installing sensors are emerging and additional manual measurements
440 could be conducted. In the future, forestry stakeholders who require accurate raster predictions could potentially facilitate
441 manual measurements or install sensors and provide the captured data to scientific organizations, which could deliver
442 spatiotemporal soil moisture predictions in return. The captured data could be made available for creating spatiotemporal
443 models of SWC, allowing for additional training data and daily raster predictions for new areas of interest, with various
444 scientific insights and practical applications.

445 **Conclusion**

446 In this study, we developed a spatiotemporal model that used multiple topographic indices, temporal variables, soil moisture
447 retrievals from ERA5-Land, and data from manual measurements to predict soil water content (SWC). Predicted values of
448 SWC were compared to rut depth data collected during four forwarder trials. Overall, the model performed well in predicting
449 rut depth, with a Kendall's τ of 0.61 for all trials. Yet, this result has to be considered with caution, since spatial covariation
450 was detected in parts. We hope, that this experience helps for future research, in which more attention to spatial covariation
451 on soils should be paid. Still, we believe that a dynamic prediction of SWC will help forest managers and machine operators
452 avoid wet areas, leading to more sustainable forest operations. Using freely available temporal information is a significant
453 improvement, as it enables more accurate and up-to-date predictions, which allow to make more informed decisions and avoid
454 potential hazards. Future work should focus on developing automated pathways for generating daily raster predictions of
455 SWC, and on generating reliable and comprehensive in-situ data. There is a need for more data on rutting and SWC, measured

456 with a sufficient spatial coverage, whether by manual measurements, the establishment of additional sensor networks, or by
457 automatic ways of capturing rut depth data through machines driving off-road, to cover more areas and different sites and
458 regions.

459 **Data availability**

460 The data used in this work will be made accessible via Zenodo

461 **Author contribution**

462 MS and DJ designed the experiments and MS and FH carried them out. MS developed the model code and performed the
463 simulations. MS prepared the manuscript with contributions from all co-authors.

464 **Competing interests**

465 The authors declare that they have no conflict of interest.

466 **Acknowledgements**

467 We acknowledge the financial support from the Eva Mayr-Stihl Stiftung for this work. We extend our gratitude to the
468 Geological Survey of Northrhine-Westphalia (Landesbetrieb NRW) for conducting the soil mapping on the experimental sites
469 and for their contributions to the field trials analysis. In particular, we would like to thank Dr. Heinz Peter Schrey, Dirk Elhaus,
470 Thilo Simon, and Rainer Janssen. Our appreciation also goes to the Forest Education Centre, Forstliches Bildungszentrum,
471 Zentrum für Wald und Holzwirtschaft, Landesbetrieb Wald und Holz NRW, Arnsberg, Germany, for their valuable support
472 during the fieldwork. Special thanks to Thilo Wagner and Thomas Späthe for their efforts in organizing the field trials, and to
473 Michael Schulte for operating the forwarder. ChatGPT (OpenAI, San Francisco, CA, USA) provided assistance in sentence
474 editing – all content was generated solely by the authors.

475 **Funding**

476 This work was supported by the cooperation project “BefahrGut” funded by the State of North Rhine-Westphalia, Germany,
477 through its Forest Education Centre, Forstliches Bildungszentrum, Zentrum für Wald und Holzwirtschaft, Landesbetrieb Wald
478 und Holz NRW, Arnsberg, Germany; by the Bio Based Industries Joint Undertaking under the European Union’s Horizon
479 2020 research and innovation program, TECH4EFFECT Knowledge and Technologies for Effective Wood Procurement—
480 project, [grant number 720757].

481

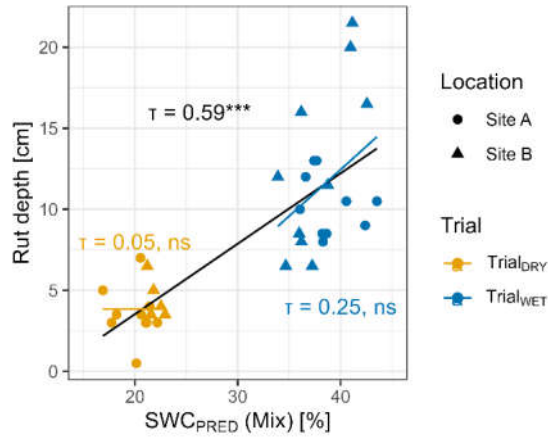
482 **5 Appendix**

483 **Appendix A**

484 To model the dataset consisting of both IMT and SSN data, the procedure described in section 2 was followed. The IMT
485 dataset was merged with a subsample of the SSN dataset, where the sample size of the SSN part was twice that of the IMT
486 dataset. This was done to prevent over-weighting of the SSN dataset. The resulting combination of IMT and SSN data was
487 called the "Mix" dataset.

488 The final model using the Mix dataset included the input variables SWC_{ERAL2} , Month, TWI, SWC_{ERAL1} , DTW025, Season,
489 DTW1 and DTW4, and achieved a τ of 0.655 ± 0.081 (which corresponded to R^2 values of 0.639 ± 0.108). Figure A1 shows
490 that the correlation between the model outputs (SWC_{PRED}) and rut depth (RD) was significant.

491 Since the models trained on the Mix dataset did not perform better than those trained on the IMT or SSN datasets, we did not
492 investigate the fused data partition any further, as one research question addressed the use of different data origins. For future
493 work, however, the fused data would provide additional information, as compared to the individual datasets.



494

Figure A1: Rut depth (RD) was determined after four passes of a forwarder, driving on two Sites (A and B), during two seasons (Trial_{WET} and Trial_{DRY}). RD was compared to SWC values predicted by a random forest model trained on data from manual measurements or captured through a continuously measuring soil sensor network ('Mix'). Correlations were evaluated using Kendall's τ and significance levels are indicated by *** for $p < 0.001$, ** for 0.001-0.01, * for 0.01-0.05, (*) for 0.05-0.10, and 'ns' for $p > 0.10$.

495

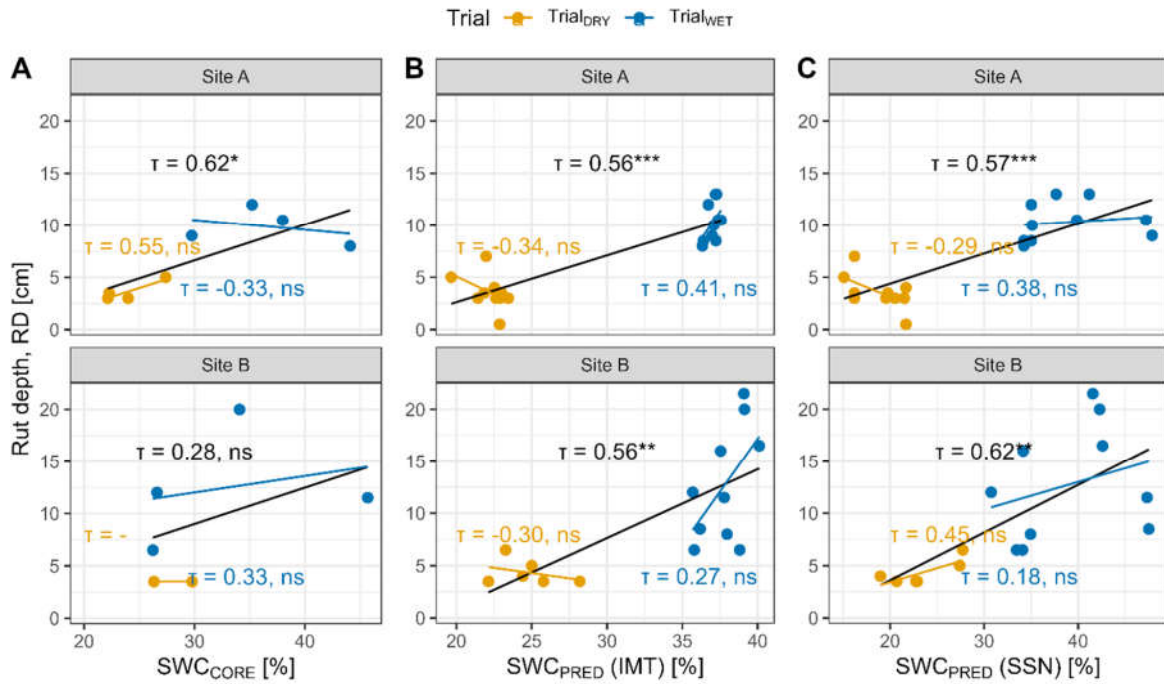
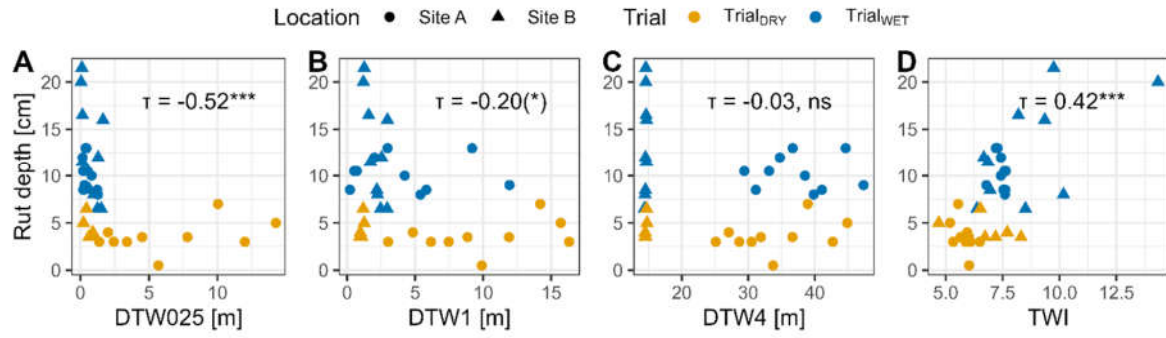


Figure B21. Rut depth (RD) was determined after four passes of a forwarder, driving on two Sites (A and B, Figure 2), during two seasons (Trial_{WET} and Trial_{DRY}, conducted under different moisture conditions). RD was compared to SWC values, determined for undisturbed soil cores (A) and SWC values predicted by a random forest model trained on manually obtained IMT measurements (B, see Figure 1) and predicted by a model trained data from a continuously measuring soil sensor network (SSN, C). Correlations were evaluated using Kendall's τ . The correlation of all values is given in black, blue and yellow show the Trials during wet and dry conditions. Significance levels are indicated by *** for $p < 0.001$, ** for 0.001-0.01, * for 0.01-0.05, (*) for 0.05-0.10, and 'ns' for $p > 0.10$.

498
499
500
501
502

Appendix C

Considering the significance of the topographic indices DTW and TWI in the development of the SWC models (Figure 4), we aimed to compare RD with both indices. Notably, RD exhibited a clear correlation with DTW025, the most conservative DTW scenario (). TWI also demonstrated a correlation with RD.



503

Figure C1: Figure 6. Rut depth (RD) was determined after four passes of a forwarder, driving on two Sites (A and B), during two conditions (Trial_{WET} and Trial_{DRY}). RD was compared to the topographic indices depth-to-water (DTW), calculated with different flow initiation areas (0.25 – 4.00 ha), and the topographic wetness index. Correlations were evaluated using Kendall's τ and significance levels are indicated by *** for $p < 0.001$, ** for 0.001-0.01, * for 0.01-0.05, (*) for 0.05-0.10, and 'ns' for $p > 0.10$.

504
505

While showing significant correlations, the nature of these static maps does not allow for the representation of current moisture conditions. This limitation was overcome when using the predicted (or observed) values of SWC.

507 **6 References**

- 508 Ågren, A., Larson, J., Paul, S. S., Laudon, H., and Lidberg, W.: Use of multiple LIDAR-derived digital terrain indices and
 509 machine learning for high-resolution national-scale soil moisture mapping of the Swedish forest landscape, *Geoderma*,
 510 404, 115280, <https://doi.org/10.1016/j.geoderma.2021.115280>, 2021.
- 511 Ågren, A., Lidberg, W., and Ring, E.: Mapping Temporal Dynamics in a Forest Stream Network—Implications for Riparian
 512 Forest Management, *Forests*, 6, 2982–3001, <https://doi.org/10.3390/f6092982>, 2015.
- 513 Ågren, A., Lidberg, W., Strömberg, M., Ogilvie, J., and Arp, P.: Evaluating digital terrain indices for soil wetness mapping –
 514 a Swedish case study, *Hydrology and Earth System Sciences*, 18, 3623–3634, <https://doi.org/10.5194/hess-18-3623-2014>,
 515 2014.
- 516 Ala-Ilomäki, J., Lindeman, H., Mola-Yudego, B., Prinz, R., Väätäinen, K., Talbot, B., and Routa, J.: The effect of bogie track
 517 and forwarder design on rut formation in a peatland, *International Journal of Forest Engineering*, 45, 1–8,
 518 <https://doi.org/10.1080/14942119.2021.1935167>, 2021.
- 519 Allman, M., Jankovský, M., Messingerová, V., and Allmanová, Z.: Soil moisture content as a predictor of soil disturbance
 520 caused by wheeled forest harvesting machines on soils of the Western Carpathians, *Journal of Forestry Research*, 28,
 521 283–289, <https://doi.org/10.1007/s11676-016-0326-y>, 2017.
- 522 Ampoorter, E., van Nevel, L., Vos, B. de, Hermy, M., and Verheyen, K.: Assessing the effects of initial soil characteristics,
 523 machine mass and traffic intensity on forest soil compaction, *Forest Ecology and Management*, 260, 1664–1676,
 524 <https://doi.org/10.1016/j.foreco.2010.08.002>, 2010.
- 525 Awaida, A. and Westervelt, J.: Geographic Resources Analysis Support System (GRASS GIS), Geographic Resources
 526 Analysis Support System (GRASS GIS) Software, USA, available at: <https://grass.osgeo.org>, 2020.
- 527 Beylich, A., Oberholzer, H.-R., Schrader, S., Höper, H., and Wilke, B.-M.: Evaluation of soil compaction effects on soil biota
 528 and soil biological processes in soils, *Soil and Tillage Research*, 109, 133–143, <https://doi.org/10.1016/j.still.2010.05.010>,
 529 2010.
- 530 Bezirksregierung Köln: Landbedeckung NRW, [https://www.bezreg-koeln.nrw.de/geobasis-nrw/produkte-und-](https://www.bezreg-koeln.nrw.de/geobasis-nrw/produkte-und-dienste/luftbild-und-satellitenbildinformationen/aktuelle-luftbild-und-3)
 531 [dienste/luftbild-und-satellitenbildinformationen/aktuelle-luftbild-und-3](https://www.bezreg-koeln.nrw.de/geobasis-nrw/produkte-und-dienste/luftbild-und-satellitenbildinformationen/aktuelle-luftbild-und-3), last access: 16 November 2023, 2023.
- 532 Bezirksregierung Köln: Digitales Geländemodell DGM1 [Digital elevation model], [https://www.bezreg-](https://www.bezreg-koeln.nrw.de/brk_internet/geobasis/hoehenmodelle/digitale_gelaendemodelle/gelaendemodell/index.html)
 533 [koeln.nrw.de/brk_internet/geobasis/hoehenmodelle/digitale_gelaendemodelle/gelaendemodell/index.html](https://www.bezreg-koeln.nrw.de/brk_internet/geobasis/hoehenmodelle/digitale_gelaendemodelle/gelaendemodell/index.html), last access: 8
 534 November 2021, 2020.
- 535 Bivand, R. S.: rgrass7: Interface Between GRASS 7 Geographical Information System and R, available at: [https://CRAN.R-](https://CRAN.R-project.org/package=rgrass7)
 536 [project.org/package=rgrass7](https://CRAN.R-project.org/package=rgrass7), 2021.
- 537 Breiman, L.: Random forests, *Machine Learning*, 45, 5–32, <https://doi.org/10.1023/A:1010933404324>, 2001.
- 538 Cambi, M., Certini, G., Neri, F., and Marchi, E.: The impact of heavy traffic on forest soils: A review, *Forest Ecology and*
 539 *Management*, 338, 124–138, <https://doi.org/10.1016/j.foreco.2014.11.022>, 2015.
- 540 Campbell, D. M.H., White, B., and Arp, P.: Modeling and mapping soil resistance to penetration and rutting using LiDAR-
 541 derived digital elevation data, *Journal of Soil and Water Conservation*, 68, 460–473,
 542 <https://doi.org/10.2489/jswc.68.6.460>, 2013.

543 Carranza, C., Nolet, C., Peziz, M., and van der Ploeg, M.: Root zone soil moisture estimation with Random Forest, *Journal of*
544 *Hydrology*, 593, 125840, <https://doi.org/10.1016/j.jhydrol.2020.125840>, 2021.

545 Cavalli, A., Francini, S., McRoberts, R. E., Falanga, V., Congedo, L., Fioravante, P. de, Maesano, M., Munafò, M., Chirici,
546 G., and Scarascia Mugnozza, G.: Estimating Afforestation Area Using Landsat Time Series and Photointerpreted
547 Datasets, *Remote Sensing*, 15, 923, <https://doi.org/10.3390/rs15040923>, 2023.

548 Chen, T., He, T., Benesty, M., Khotilovich, V., Tang, Y., Cho, H., Chen, K., Mitchell, R., Cano, I., Zhou, T., Li, M., Xie, J.,
549 Lin, M., Geng, Y., and Li, Y.: xgboost: Extreme Gradient Boosting, <https://CRAN.R-project.org/package=xgboost>, last
550 access: 9 November 2021, 2021.

551 Copernicus Climate Change Service: ERA5-Land hourly data from 2001 to present, 2019.

552 Crawford, L. J., Heinse, R., Kimsey, M. J., and Page-Dumroese, D. S.: Soil Sustainability and Harvest Operations, General
553 Technical Report RMRS, <https://doi.org/10.2737/RMRS-GTR-421>, 2021.

554 Curzon, M. T., Slesak, R. A., Palik, B. J., and Schwager, J. K.: Harvest impacts to stand development and soil properties
555 across soil textures: 25-year response of the aspen Lake States LTSP installations, *Forest Ecology and Management*, 504,
556 119809, <https://doi.org/10.1016/j.foreco.2021.119809>, 2022.

557 D'Acqui, L. P., Certini, G., Cambi, M., and Marchi, E.: Machinery's impact on forest soil porosity, *Journal of Terramechanics*,
558 91, 65–71, <https://doi.org/10.1016/j.jterra.2020.05.002>, 2020.

559 DeArmond, D., Ferraz, J., and Higuchi, N.: Natural Recovery of Skid Trails. A Review, *Canadian Journal of Forest Research*,
560 <https://doi.org/10.1139/cjfr-2020-0419>, 2021.

561 Eijkelkamp Agrisearch Equipment: User Manual for the Moisture Meter type HH2,
562 https://www.eijkelkamp.com/download.php?file=M1142602e_Soil_moisture_meter_flab.pdf, last access: 7 August
563 2020, 2013.

564 Eliasson, L.: Effects of forwarder tyre pressure on rut formation and soil compaction, *Silva Fennica*, 39, 549–557,
565 <https://doi.org/10.14214/sf.366>, available at: <http://www.metla.fi/silvafennica/full/sf39/sf394549.pdf>, 2005.

566 Finnish Meteorological Institute: Harvester Seasons,
567 https://harvesterseasons.com/HarvesterSeasons_Description2pager_v2.pdf, last access: 8 November 2023, 2023.

568 Fjeld, D., Persson, M., Fransson, J. E.S., Bjerketvedt, J., and Bråthen, M.: Modelling forest road trafficability with satellite-
569 based soil moisture variables, *International Journal of Forest Engineering*, 35, 93–104,
570 <https://doi.org/10.1080/14942119.2023.2276628>, 2024.

571 Francesca, V., Osvaldo, F., Stefano, P., and Paola, R. P.: Soil Moisture Measurements: Comparison of Instrumentation
572 Performances, *J. Irrig. Drain Eng.*, 136, 81–89, [https://doi.org/10.1061/\(ASCE\)0733-9437\(2010\)136:2\(81\)](https://doi.org/10.1061/(ASCE)0733-9437(2010)136:2(81)), 2010.

573 Grüll, M.: Den Waldboden schonen–Vorsorgender Bodenschutz beim Einsatz von Holzerntetechnik [Soil protection in forest
574 operations], *Eberswalder Forstliche Schriftenreihe*, 47, 37–44, available at:
575 [https://www.waldwissen.net/assets/technik/holzernte/boden/lfe_bodenschutz/download/lfe_bodenschutz_originalbeitrag](https://www.waldwissen.net/assets/technik/holzernte/boden/lfe_bodenschutz/download/lfe_bodenschutz_originalbeitrag.pdf)
576 [.pdf](https://www.waldwissen.net/assets/technik/holzernte/boden/lfe_bodenschutz/download/lfe_bodenschutz_originalbeitrag.pdf), 2011.

577 Guo, M., Li, J., Sheng, C., Xu, J., and Wu, L.: A Review of Wetland Remote Sensing, *Sensors (Basel, Switzerland)*, 17,
578 <https://doi.org/10.3390/s17040777>, 2017.

579 Hamner, B. and Frasco, M.: Metrics: Evaluation Metrics for Machine Learning, available at: [https://CRAN.R-](https://CRAN.R-project.org/package=Metrics)
580 [project.org/package=Metrics](https://CRAN.R-project.org/package=Metrics), 2018.

581 Hansson, L., Šimůnek, J., Ring, E., Bishop, K., and Gärdenäs, A. I.: Soil Compaction Effects on Root-Zone Hydrology and
582 Vegetation in Boreal Forest Clearcuts, *Soil Sci. Soc. Am. j.*, 83, 239, <https://doi.org/10.2136/sssaj2018.08.0302>, 2019.

583 Hauglin, M., Rahlf, J., Schumacher, J., Astrup, R., and Breidenbach, J.: Large scale mapping of forest attributes using
584 heterogeneous sets of airborne laser scanning and National Forest Inventory data, *Forest Ecosystems*, 8, 65,
585 <https://doi.org/10.1186/s40663-021-00338-4>, 2021.

586 Heppelmann, J. B., Talbot, B., Antón Fernández, C., and Astrup, R.: Depth-to-water maps as predictors of rut severity in fully
587 mechanized harvesting operations, *International Journal of Forest Engineering*, 33, 108–118,
588 <https://doi.org/10.1080/14942119.2022.2044724>, 2022.

589 Heubaum, F.: Bodenschutz im Staatsbetrieb Sachsenforst [Soil protection]: Projekte zur Technologieerprobung, Staatsbetrieb
590 Sachsenforst, https://www.sbs.sachsen.de/download/Bodenschutz_Projekte_2015_09_30.pdf, last access: 5 November
591 2021, 2015.

592 Hijmans, R. J.: raster: Geographic Data Analysis and Modeling, available at: <https://CRAN.R-project.org/package=raster>,
593 2020.

594 Hillel, D.: Environmental soil physics: Fundamentals, applications, and environmental considerations, Elsevier, San Diego,
595 California, 1998.

596 Hoffmann, S., Schönauer, M., Heppelmann, J., Asikainen, A., Cacot, E., Eberhard, B., Hasenauer, H., Ivanovs, J., Jaeger, D.,
597 Lazdins, A., Mohtashami, S., Moskalik, T., Nordfjell, T., Stereńczak, K., Talbot, B., Uusitalo, J., Vuillermoz, M., and
598 Astrup, R.: Trafficability Prediction Using Depth-to-Water Maps: the Status of Application in Northern and Central
599 European Forestry, *Curr Forestry Rep*, 338, 124, <https://doi.org/10.1007/s40725-021-00153-8>, 2022.

600 Horn, R., Vossbrink, J., Peth, S., and Becker, S.: Impact of modern forest vehicles on soil physical properties, *Forest Ecology
601 and Management*, 248, 56–63, <https://doi.org/10.1016/j.foreco.2007.02.037>, 2007.

602 James, S. E., Pärtel, M., Wilson, S. D., and Peltzer, D. A.: Temporal heterogeneity of soil moisture in grassland and forest,
603 *Journal of Ecology*, 234–239, 2003.

604 Jones, M.-F. and Arp, P.: Soil Trafficability Forecasting, *Open Journal of Forestry*, 9, 296–322,
605 <https://doi.org/10.4236/ojf.2019.94017>, 2019.

606 Jones, M.-F. and Arp, P.: Relating Cone Penetration and Rutting Resistance to Variations in Forest Soil Properties and Daily
607 Moisture Fluctuations, *Open Journal of Soil Science*, 07, 149–171, <https://doi.org/10.4236/ojss.2017.77012>, 2017.

608 Kelliher, F. M., Leuning, R., and Schulze, E. D.: Evaporation and canopy characteristics of coniferous forests and grasslands,
609 *Oecologia*, 95, 153–163, <https://doi.org/10.1007/BF00323485>, 1993.

610 Kempainen, J., Niittynen, P., Riihimäki, H., and Luoto, M.: Modelling soil moisture in a high-latitude landscape using LiDAR
611 and soil data, *Earth Surf. Process. Landforms*, 43, 1019–1031, <https://doi.org/10.1002/esp.4301>, 2018.

612 Koen Hufkens, Reto Stauffer, and Elio Campitelli: *khufkens/ecmwfr: ecmwfr*, Zenodo, 2019.

613 Kristensen, J. A., Balstrøm, T., Jones, R. J. A., Jones, A., Montanarella, L., Panagos, P., and Breuning-Madsen, H.:
614 Development of a harmonised soil profile analytical database for Europe: a resource for supporting regional soil
615 management, *SOIL*, 5, 289–301, <https://doi.org/10.5194/soil-5-289-2019>, 2019.

616 Kuglerová, L., Hasselquist, E. M., Richardson, J. S., Sponseller, R. A., Kreuzweiser, D. P., and Laudon, H.: Management
617 perspectives on *Aqua incognita* Connectivity and cumulative effects of small natural and artificial streams in boreal
618 forests, *Hydrological Processes*, 31, 4238–4244, <https://doi.org/10.1002/hyp.11281>, 2017.

619 Kursa, M. B. and Rudnicki, W. R.: Feature Selection with the Boruta Package, *J. Stat. Soft.*, 36,
620 <https://doi.org/10.18637/jss.v036.i11>, 2010.

621 Labelle, E. R. and Jaeger, D.: Management Implications of Using Brush Mats for Soil Protection on Machine Operating Trails
622 during Mechanized Cut-to-Length Forest Operations, *Forests*, 10, 19, <https://doi.org/10.3390/f10010019>, 2018.

623 Labelle, E. R., Poltorak, B. J., and Jaeger, D.: The role of brush mats in mitigating machine-induced soil disturbances: An
624 assessment using absolute and relative soil bulk density and penetration resistance, *Canadian Journal of Forest Research*,
625 49, 164–178, <https://doi.org/10.1139/cjfr-2018-0324>, 2019.

626 Lal, P., Singh, G., Das, N. N., Colliander, A., and Entekhabi, D.: Assessment of ERA5-Land Volumetric Soil Water Layer
627 Product Using In Situ and SMAP Soil Moisture Observations, *IEEE Geosci. Remote Sensing Lett.*, 19, 1–5,
628 <https://doi.org/10.1109/LGRS.2022.3223985>, 2022.

629 Larson, J., Lidberg, W., Ågren, A. M., and Laudon, H.: Predicting soil moisture conditions across a heterogeneous boreal
630 catchment using terrain indices, 26, 2022.

631 Leach, J. A., Lidberg, W., Kuglerová, L., Peralta-Tapia, A., Ågren, A., and Laudon, H.: Evaluating topography-based
632 predictions of shallow lateral groundwater discharge zones for a boreal lake-stream system, *Water Resources Research*,
633 53, 5420–5437, <https://doi.org/10.1002/2016WR019804>, 2017.

634 Lidberg, W., Nilsson, M., and Ågren, A.: Using machine learning to generate high-resolution wet area maps for planning
635 forest management: A study in a boreal forest landscape, *Ambio*, 49, 475–486, <https://doi.org/10.1007/s13280-019-01196-9>, 2020.

637 Mattila, U. and Tokola, T.: Terrain mobility estimation using TWI and airborne gamma-ray data, *Journal of environmental*
638 *management*, 232, 531–536, <https://doi.org/10.1016/j.jenvman.2018.11.081>, 2019.

639 McNabb, D. H., Startsev, A. D., and Nguyen, H.: Soil Wetness and Traffic Level Effects on Bulk Density and Air-Filled
640 Porosity of Compacted Boreal Forest Soils, *Soil Science Society of America Journal*, 65, 1238–1247,
641 <https://doi.org/10.2136/sssaj2001.6541238x>, 2001.

642 Mohtashami, S., Eliasson, L., Jansson, G., and Sonesson, J.: Influence of soil type, cartographic depth-to-water, road
643 reinforcement and traffic intensity on rut formation in logging operations: a survey study in Sweden, *Silva Fennica*, 51,
644 <https://doi.org/10.14214/sf.2018>, 2017.

645 Moore, I. D., Grayson, R. B., and Ladson, A. R.: Digital terrain modelling: A review of hydrological, geomorphological, and
646 biological applications, *Hydrol. Process.*, 5, 3–30, <https://doi.org/10.1002/hyp.3360050103>, 1991.

647 Muñoz-Sabater, J., Dutra, E., Agustí-Panareda, A., Albergel, C., Arduini, G., Balsamo, G., Boussetta, S., Choulga, M.,
648 Harrigan, S., Hersbach, H., Martens, B., Miralles, D. G., Piles, M., Rodríguez-Fernández, N. J., Zsoter, E., Buontempo,
649 C., and Thépaut, J.-N.: ERA5-Land: a state-of-the-art global reanalysis dataset for land applications, *Earth Syst. Sci. Data*,
650 13, 4349–4383, <https://doi.org/10.5194/essd-13-4349-2021>, 2021.

651 Murphy, P. N. C., Ogilvie, J., Meng, F.-R., White, B., Bhatti, J. S., and Arp, P.: Modelling and mapping topographic variations
652 in forest soils at high resolution: A case study, *Ecological Modelling*, 222, 2314–2332,
653 <https://doi.org/10.1016/j.ecolmodel.2011.01.003>, 2011.

654 Murphy, P. N. C., Ogilvie, J., and Arp, P.: Topographic modelling of soil moisture conditions: A comparison and verification
655 of two models, *European Journal of Soil Science*, 60, 94–109, <https://doi.org/10.1111/j.1365-2389.2008.01094.x>, 2009.

656 Murphy, P. N. C., Ogilvie, J., Connor, K., and Arp, P.: Mapping wetlands: A comparison of two different approaches for New

657 Brunswick, Canada, *WETLANDS*, 27, 846–854, [https://doi.org/10.1672/0277-5212\(2007\)27\[846:MWACOT\]2.0.CO;2](https://doi.org/10.1672/0277-5212(2007)27[846:MWACOT]2.0.CO;2),
658 2007.

659 Oliveira, V. A., Rodrigues, A. F., Morais, M. A. V., Terra, M. d. C. N. S., Guo, L., and Mello, C. R.: Spatiotemporal modelling
660 of soil moisture in an Atlantic forest through machine learning algorithms, *Eur J Soil Sci*, 72, 1969–1987,
661 <https://doi.org/10.1111/ejss.13123>, 2021.

662 Peng, J., Albergel, C., Balenzano, A., Brocca, L., Cartus, O., Cosh, M. H., Crow, W. T., Dabrowska-Zielinska, K., Dadson,
663 S., Davidson, M. W.J., Rosnay, P. de, Dorigo, W., Gruber, A., Hagemann, S., Hirschi, M., Kerr, Y. H., Lovergine, F.,
664 Mahecha, M. D., Marzahn, P., Mattia, F., Musial, J. P., Preuschmann, S., Reichle, R. H., Satalino, G., Silgram, M., van
665 Bodegom, P. M., Verhoest, N. E.C., Wagner, W., Walker, J. P., Wegmüller, U., and Loew, A.: A roadmap for high-
666 resolution satellite soil moisture applications – confronting product characteristics with user requirements, *Remote
667 Sensing of Environment*, 252, 112162, <https://doi.org/10.1016/j.rse.2020.112162>, 2021.

668 Picchio, R., Latterini, F., Mederski, P. S., Tocci, D., Venanzi, R., Stefanoni, W., and Pari, L.: Applications of GIS-Based
669 Software to Improve the Sustainability of a Forwarding Operation in Central Italy, *Sustainability*, 12, 5716,
670 <https://doi.org/10.3390/su12145716>, 2020.

671 Poltorak, B. J., Labelle, E. R., and Jaeger, D.: Soil displacement during ground-based mechanized forest operations using
672 mixed-wood brush mats, *Soil and Tillage Research*, 179, 96–104, <https://doi.org/10.1016/j.still.2018.02.005>, 2018.

673 Quinn, P., Beven, K., Chevallier, P., and Planchon, O.: The prediction of hillslope flow paths for distributed hydrological
674 modelling using digital terrain models, *Hydrol. Process.*, 5, 59–79, <https://doi.org/10.1002/hyp.3360050106>, 1991.

675 R Core Team: R: A Language and Environment for Statistical Computing, The R Foundation for Statistical Computing,
676 Vienna, Austria, 2023.

677 Ring, E., Ågren, A., Bergkvist, I., Finér, L., Johansson, F., and Högbom, L.: A guide to using wet area maps in forestry: En
678 guide för hur man kan använda markfuktighetskarter i skogsbruket, ARBETSRAPPORT 1051-2020, Uppsala, Sweden,
679 2022.

680 Schönauer, M. and Maack, J.: R-code for calculating depth-to-water (DTW) maps using GRASS GIS (Version v1), Zenodo,
681 <https://doi.org/10.5281/zenodo.5638518>, 2021.

682 Schönauer, M., Prinz, R., Väättäinen, K., Astrup, R., Pszenny, D., Lindeman, H., and Jaeger, D.: Spatio-temporal prediction
683 of soil moisture using soil maps, topographic indices and SMAP retrievals, *International Journal of Applied Earth
684 Observation and Geoinformation*, 108, 102730, <https://doi.org/10.1016/j.jag.2022.102730>, 2022.

685 Schönauer, M., Hoffmann, S., Maack, J., Jansen, M., and Jaeger, D.: Comparison of Selected Terramechanical Test
686 Procedures and Cartographic Indices to Predict Rutting Caused by Machine Traffic during a Cut-to-Length Thinning
687 Operation, *Forests*, 12, 113, <https://doi.org/10.3390/f12020113>, 2021a.

688 Schönauer, M., Väättäinen, K., Prinz, R., Lindeman, H., Pszenny, D., Jansen, M., Maack, J., Talbot, B., Astrup, R., and Jaeger,
689 D.: Spatio-temporal prediction of soil moisture and soil strength by depth-to-water maps, *International Journal of Applied
690 Earth Observation and Geoinformation*, 105, 102614, <https://doi.org/10.1016/j.jag.2021.102614>, available at:
691 <https://www.sciencedirect.com/science/article/pii/S0303243421003214>, 2021b.

692 Sirén, M., Salmivaara, A., Ala-Ilomäki, J., Launiainen, S., Lindeman, H., Uusitalo, J., Sutinen, R., and Hänninen, P.:
693 Predicting forwarder rut formation on fine-grained mineral soils, *Scandinavian Journal of Forest Research*, 34, 145–154,
694 <https://doi.org/10.1080/02827581.2018.1562567>, 2019.

695 Sørensen, R. and Seibert, J.: Effects of DEM resolution on the calculation of topographical indices: TWI and its components,
696 *Journal of Hydrology*, 347, 79–89, <https://doi.org/10.1016/j.jhydrol.2007.09.001>, 2007.

697 Suvinen, A. and Saarilahti, M.: Measuring the mobility parameters of forwarders using GPS and CAN bus techniques, *Journal*
698 *of Terramechanics*, 43, 237–252, <https://doi.org/10.1016/j.jterra.2005.12.005>, 2006.

699 Tromp-van Meerveld, H. J. and McDonnell, J. J.: On the interrelations between topography, soil depth, soil moisture,
700 transpiration rates and species distribution at the hillslope scale, *Advances in Water Resources*, 29, 293–310,
701 <https://doi.org/10.1016/j.advwatres.2005.02.016>, 2006.

702 Uusitalo, J., Ala-Ilomäki, J., Lindeman, H., Toivio, J., and Sirén, M.: Predicting rut depth induced by an 8-wheeled forwarder
703 in fine-grained boreal forest soils, *Annals of forest science*, 77, <https://doi.org/10.1007/s13595-020-00948-y>, 2020.

704 Uusitalo, J., Ala-Ilomäki, J., Lindeman, H., Toivio, J., and Sirén, M.: Modelling soil moisture – soil strength relationship of
705 fine-grained upland forest soils, *Silva Fennica*, 53, <https://doi.org/10.14214/sf.10050>, 2019.

706 Vega-Nieva, D. J., Murphy, P. N. C., Castonguay, M., Ogilvie, J., and Arp, P.: A modular terrain model for daily variations
707 in machine-specific forest soil trafficability, *Canadian Journal of Soil Science*, 89, 93–109,
708 <https://doi.org/10.4141/CJSS06033>, 2009.

709 Walker, J. P., Willgoose, G. R., and Kalma, J. D.: In situ measurement of soil moisture: a comparison of techniques, *Journal*
710 *of Hydrology*, 293, 85–99, <https://doi.org/10.1016/j.jhydrol.2004.01.008>, 2004.

711 White, B., Ogilvie, J., Campbell, D. M.H., Hiltz, D., Gauthier, B., Chisholm, H. K., Wen, H. K., Murphy, P. N. C., and Arp,
712 P.: Using the Cartographic Depth-to-Water Index to Locate Small Streams and Associated Wet Areas across Landscapes,
713 *Canadian Water Resources Journal*, 37, 333–347, <https://doi.org/10.4296/cwrj2011-909>, 2012.

714 Wright, M. N. and Ziegler, A.: ranger: A Fast Implementation of Random Forests for High Dimensional Data in C++ and R,
715 *J. Stat. Soft.*, 77, <https://doi.org/10.18637/jss.v077.i01>, 2017.

716